SUPPORTING INFORMATION

High Symmetry or Low Symmetry, It Is a Question − High Performance Dy(III) Single-ion Magnets by Electrostatic Potential Design

Wen-Bin Sun, [a,b] Peng-Fei Yan,[b] Shang-Da Jiang,[a] Bing-Wu Wang, *[a] Yi-Quan Zhang, [a] Hong-Feng Li, [b] Peng Chen, [b] Zhe-Ming Wang [a] and Song Gao*[a]

[a] Beijing National Laboratory of Molecular Science State Key Laboratory of Rare Earth Materials Chemistry and Applications, College of Chemistry and Molecular Engineering, Peking University Beijing 100871, P. R. China. Fax: (+86) 10-6275-1708; Tel: (+86) 10-6276-7569; E-mail: wangbw@pku.edu.cn and gaosong@pku.edu.cn

[b] Key Laboratory of Functional Inorganic Material Chemistry Ministry of Education, Heilongjiang University, Harbin 150080, P. R. China.

Table S1 Crystallographic data for **1-4**

	1	**2**	**3**	**4**
Empirical formula	$C_{44}H_{36}Cl_3DyN_4O_{10}Zn_2$	$C_{45}H_{44}Br_3DyN_4O_{11}Zn_2$	$C_{44}H_{38}Br_5DyN_4O_9Zn_3$	$C_{44}H_{48}Cl_3DyN_4O_8Zn_2$
FW (g mol^{-1})	1180.40	1349.81	1524.95	1160.45
Crystal system	Monoclinic	Triclinic	Monoclinic	Monoclinic
Space group	C2/c	P-1	*P*21/c	C 2/c
Temperature(K)	293(2)	293(2)	293(2)	293(2)
a (Å)	16.203(3)	10.6840(4)	12.6367(6)	16.2823(6)
b (Å)	22.757(5)	15.3563(7)	16.8613(8)	23.8976(10)
c (Å)	14.315(3)	16.5041(6)	23.4058(12)	14.0704(6)
α (°)	90.00	92.185(4)	90.00	90.00
β (°)	104.77(3)	108.231(4)	104.117(5)	104.843(4)
γ (°)	90.00	99.113(4)	90.00	90.00
V (Å^3)	5104.0(18)	2528.26(18)	4836.5(4)	5292.2(4)
ρ_{cacd} (Mg cm^{-3})	1.515	1.773	1.940	1.456
μ (mm^{-1})	2.590	4.833	6.116	2.496
F (000)	2307	1322	2732	2324
Collected reflections	23835	24055	34215	11638
Independent reflections	5794	11499	10425	5887
Rint	0.0620	0.0978	0.0713	0.0350
R1 [I > 2σ(I)]	0.0402	0.0811	0.0517	0.0366

wR2 (all data)	0.0976	0.2321	0.1346	0.0947
Goodness of fit on F^2	1.037	1.033	1.060	1.081

Table S2 Continuous Shape Measures (CShMs) of the coordination geometry for Dy(III) ion in compounds **1**-**4** (S values calculated with the Shape program). The *S* values indicated the proximity to the ideal polyhedron, thus, an $S = 0$ corresponds to the non-distorted polyhedron. The three closer ideal geometries to the real complexes are listed

	1	**2**	**3**	**4**
CSAPR-9	3.437	2.841	2.115	3.452
TCTPR-9	3.566	3.625	2.124	3.592
MFF-9	3.321	2.635	2.461	3.280
CSAPR-9	C4v	Spherical capped square antiprism		
TCTPR-9	D3h	Spherical tricapped trigonal prism		
MFF-9	Cs	Muffin		

Table S3 Deviations (Å) from the ideal plane defined by five coordination atoms. The positive value denotes that the oxygen atom is located on the same side of the Ln atom, whereas a negative value denotes that the atom is located on the opposite side

coordination atoms	**1**	**4**	coordination atoms	**2**	**3**
Cl2	0.0000	-0.0000	O9	0.1446	0.6312
O4	-0.1324	-0.1443	O4	-0.2430	-0.0207
O3’	0.2293	0.2279	O8	0.1694	-0.2311
O3	-0.2293	-0.2279	O3	-0.2161	0.3387
O4’	0.1324	0.1443	O7	0.0481	-0.4163

Table S4 Mulliken charges of atoms in the ground state of **1**-**4** obtained at CASSCF/ANO-RCC level of theory

Coordination Atoms			**1**	**2**	**3**	**4**
Phenoxyl oxygen atoms		O	-1.0590	-1.0670	-1.0646	-1.0727
		O	-1.0332	-1.0361	-1.0461	-1.0322
		O	-1.0592	-1.0665	-1.0644	-1.0728
		O	-1.0332	-1.0384	-1.0493	-1.0318
Average			-1.0462	-1.0520	-1.0561	-1.0523
Forming the hard plane	Methoxyl oxygen atoms	O	-0.8146	-0.8358	-0.8336	-0.8457
		O	-0.8345	-0.8563	-0.8320	-0.8150
		O	-0.8146	-0.8479	-0.8476	-0.8459
		O	-0.8346	-0.8457	-0.8331	-0.8152
	Cl for **1** and **4**, O for **2** and **3**		-0.7780	-0.7416	-0.5550	-0.7850
	Average		-0.8153	-0.8255	-0.7803	-0.8214

Table S5 The orientation of local magnetic moment in **1-4** (dark blue arrow), *g* values and calculated energy difference (ΔE, cm^{-1}) between the ground state and first excited state

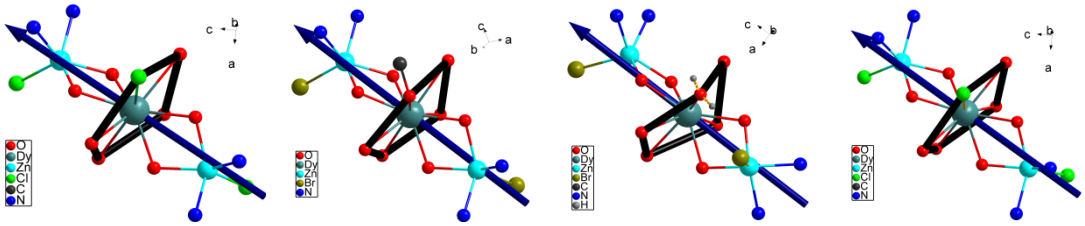

	1	**2**	**3**	**4**
g_x	0.0000	0.0012	0.0023	0.0002
g_y	0.0002	0.0018	0.0036	0.0005
g_z	19.9615	19.8462	19.7884	19.9658
ΔE	355.6	351.8	313.0	351.9

Table S6 The curves are fitted by the modified Arrhenius relationship the Raman process is taken account

$1/\tau = CT^n + \tau_0^{-1}\exp(-U_{eff}/\kappa_B T)$

dc filed	**C** ($s^{-1}\cdot K^{-n}$)	**n**	τ_0 (s)	U_{eff}/κ_B (K)
0 Oe	7.9×10^{-5}	4.4	7.4×10^{-11}	430
1000 Oe	1.1×10^{-7}	6.5	1.3×10^{-11}	481
Zero field for dilution sample	1.0×10^{-6}	5.8	7.0×10^{-11}	434

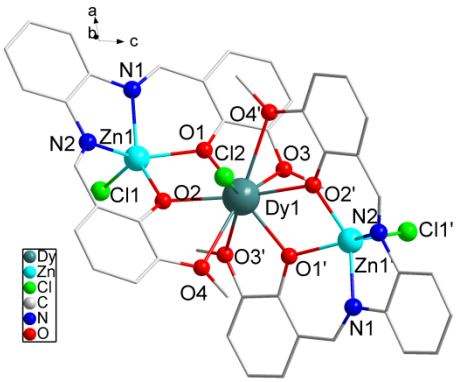

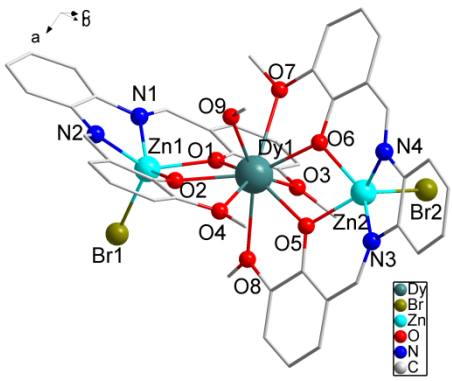

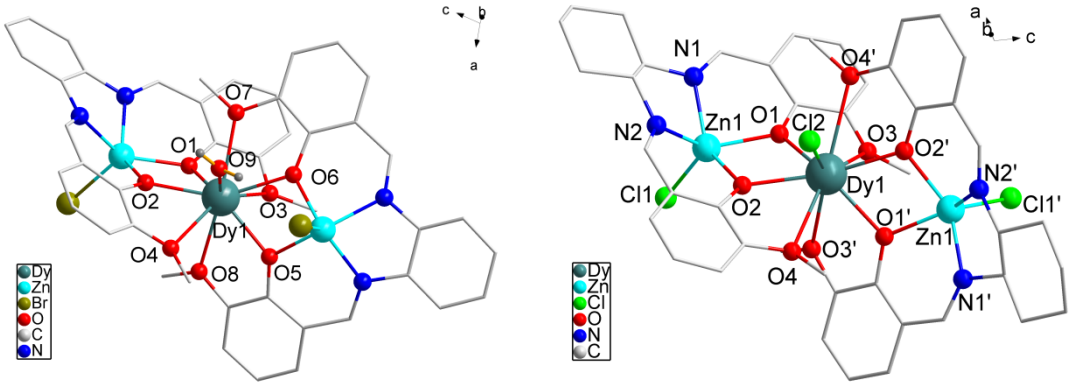

Fig. S1 The structure for **1** (top left), **2** (top right), **3** (bottom left), **4** (bottom right), hydrogen atoms and counter anions are omitted for clarity.

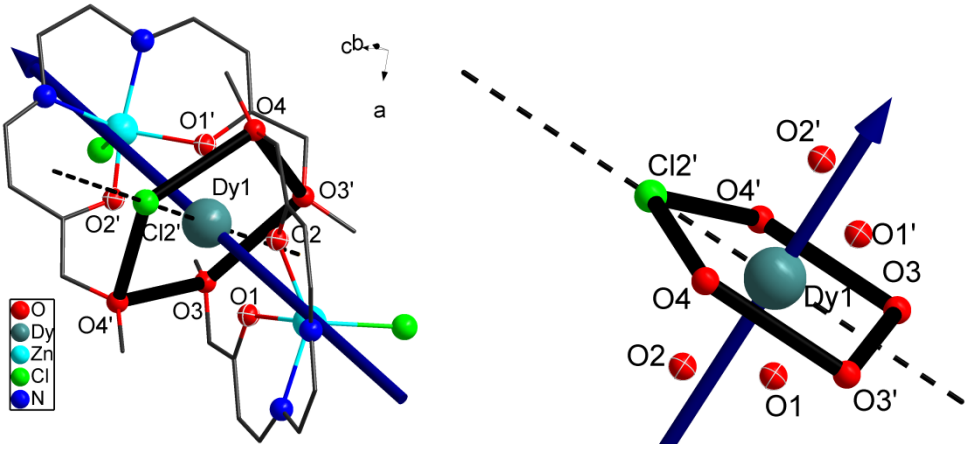

Fig. S2 The local coordination geometry of Dy(III) center and the orientation of local magnetic moment in **1** (dark blue arrow), the black dashed line represents the C_2 symmetry axis, the H atoms and benzene moiety are omitted for clearity. The thick black ring is composed of four methoxyl oxygen atoms and one chlorine atoms which display the lowest electronic density. In contrast, the phenoxyl oxygen atoms O1, O2, O1' and O2' have the highest electronic density (see table S4).

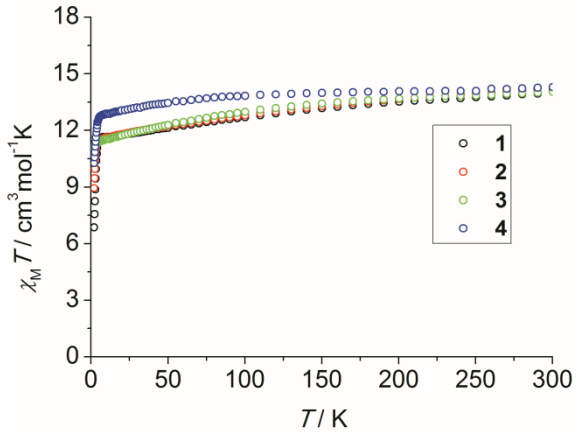

Fig. S3 Temperature dependence of $\chi_M T$ and $\chi_M{}^{-1}$ measured at 1000 Oe for **1-4**.

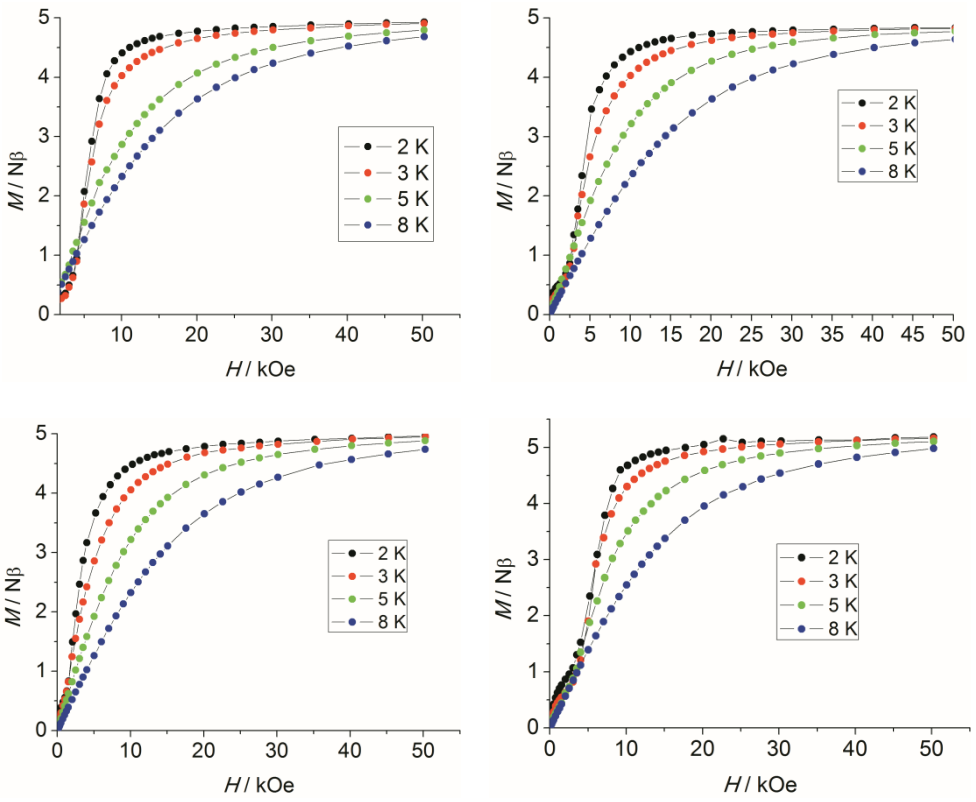

Fig. S4 The field dependence of magnetization at 2, 3, 5 and 8 K for **1** (top left), **2** (top right), **3** (bottom left), **4** (bottom right).

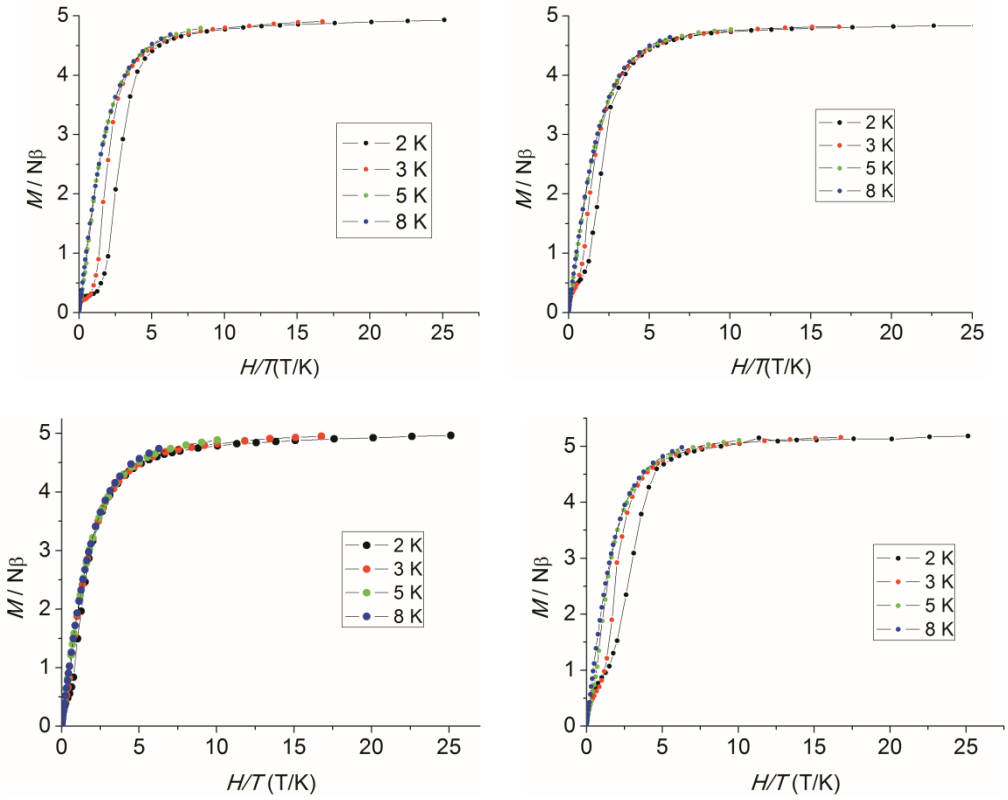

Fig. S5 Magnetization data for complex **1** at 2, 3, 5 and 8 K for **1** (top left), **2** (top right), **3** (bottom left), **4** (bottom right).

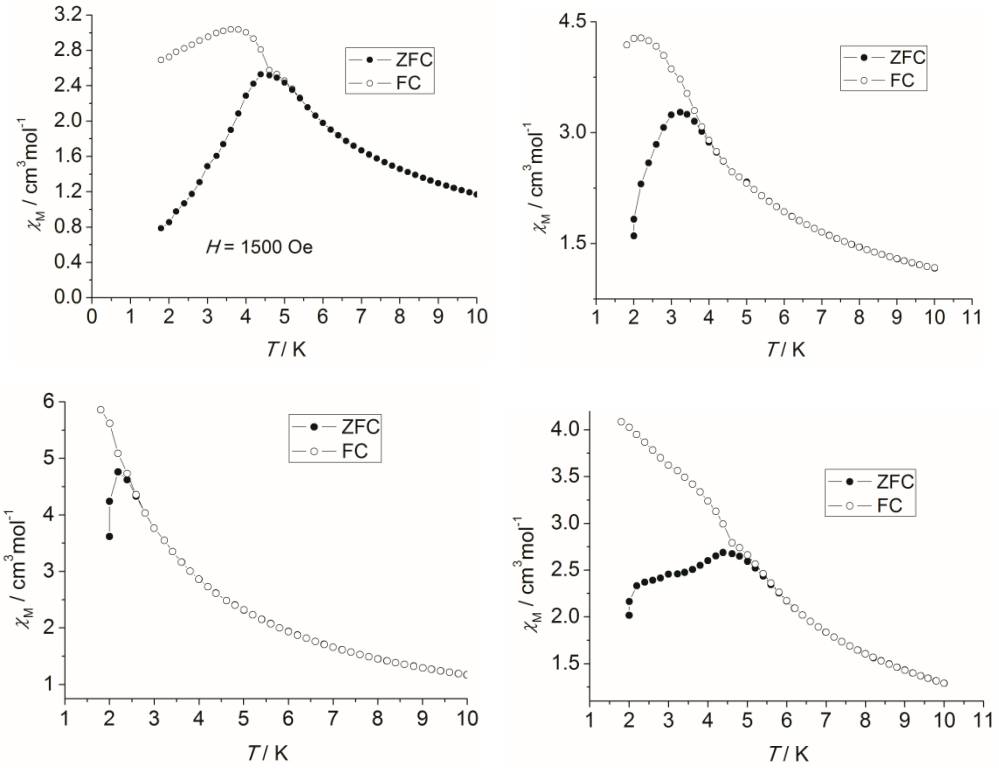

Fig. S6 The zero-field-cooled (ZFC) and field-cooled (FC) susceptibilities at 1500 Oe field for **1** (top left), **2** (top right), **3** (bottom left), **4** (bottom right). The divergence temperature of ZFC/FC is usually dependent on the external field during the measurement for a lanthanide SIM for the strong quantum tunneling of magnetization. In the plot of hysteresis, the open of the loop becomes larger and then decrease gradually with the increasing of external field, which could usually be found for lanthanide-based SIMs.

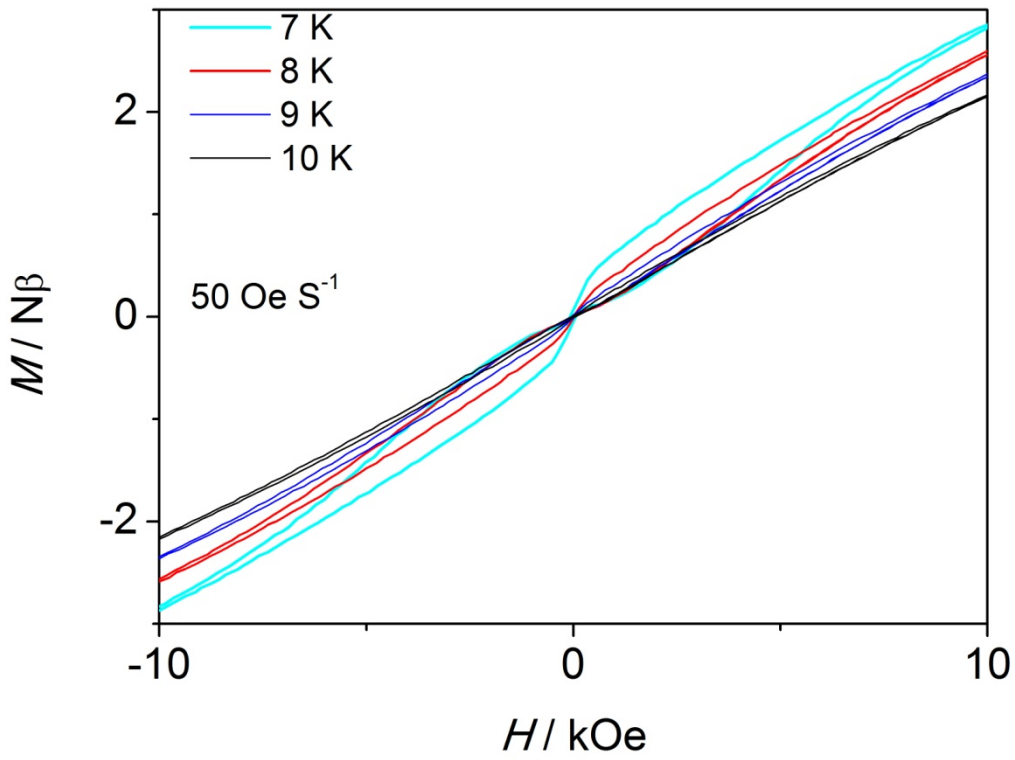

Fig. S7 Hysteresis loops at different temperatures recorded on a Quantum Design PPMS magnetometer with a sweep rate of 0.005 $T \cdot s^{-1}$ for **1**.

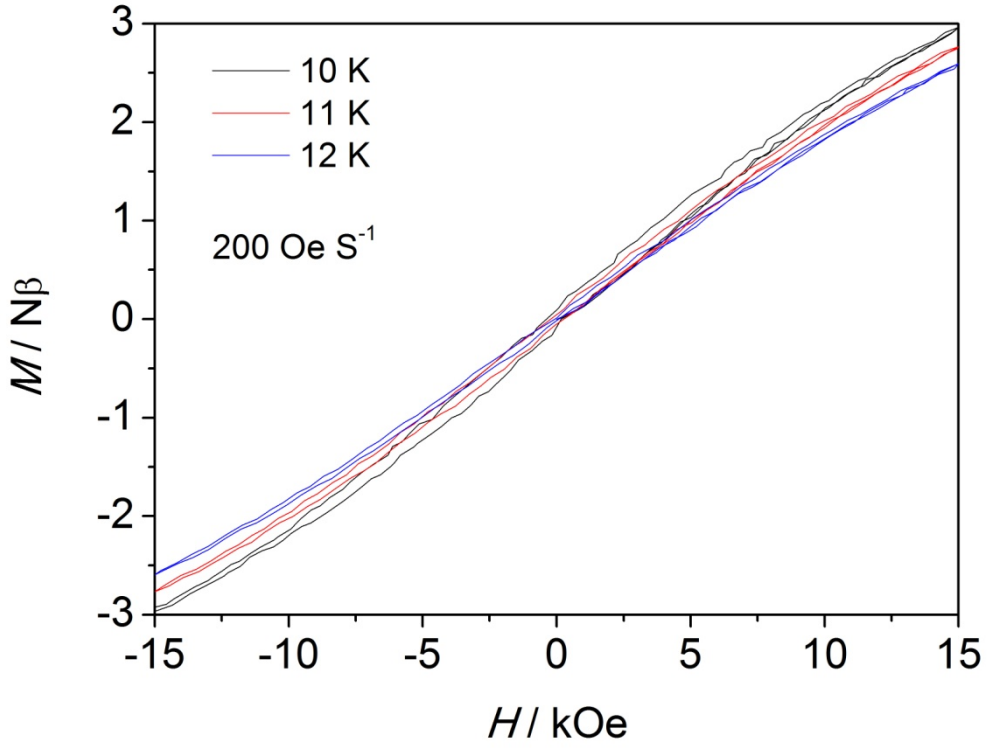

Fig. S8 Hysteresis loops at different temperatures recorded on a Quantum Design PPMS magnetometer with a sweep rate of 0.020 $T \cdot s^{-1}$ for **1**.

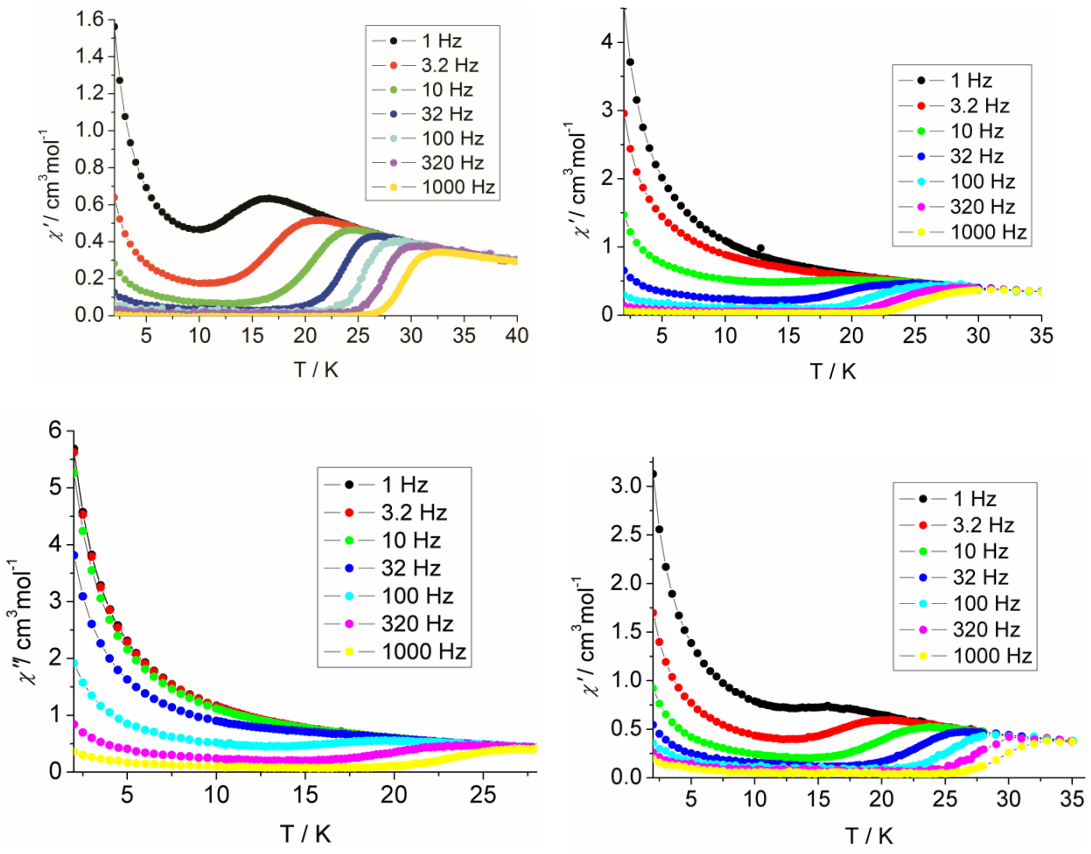

Fig. S9 The temperature dependence of the in-phase susceptibility (χ') plots of **1** (top left), **2** (top right), **3** (bottom left), **4** (bottom right), between 1 and 1000 Hz under zero dc field.

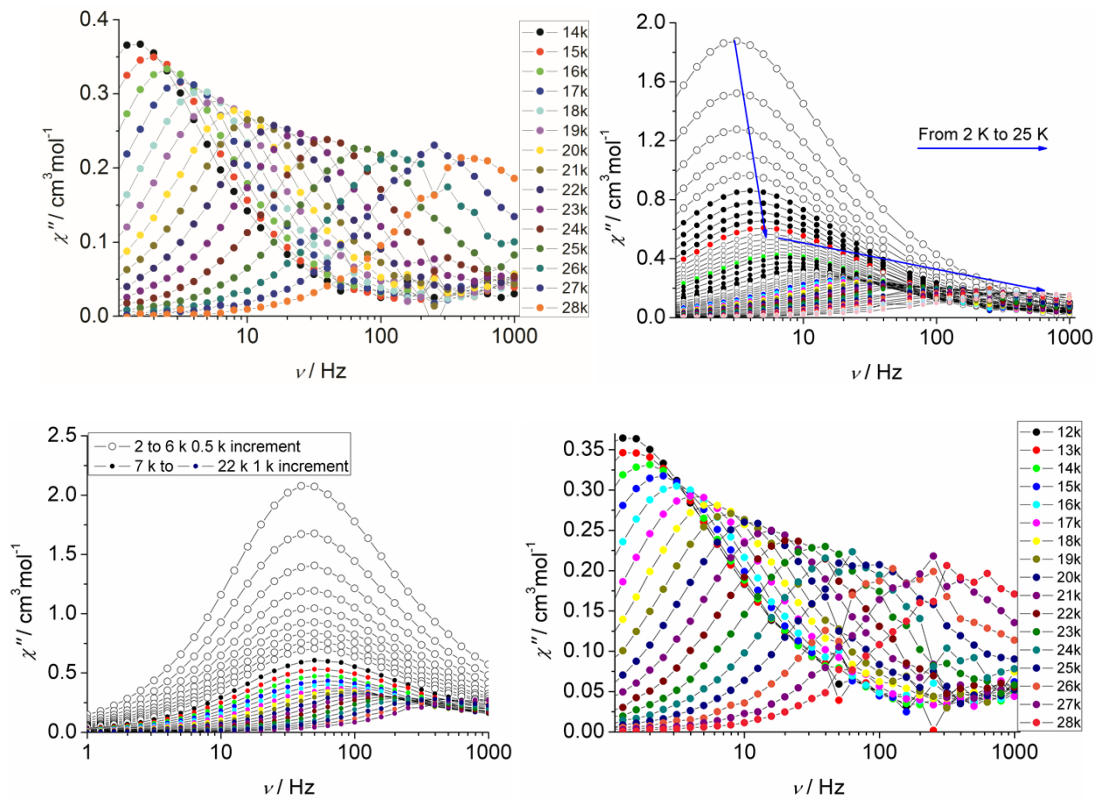

Fig. S10 The frequency dependence of the out-of-phase susceptibility (χ'') plots of **1** (top left), **2** (top right), **3** (bottom left), **4** (bottom right).

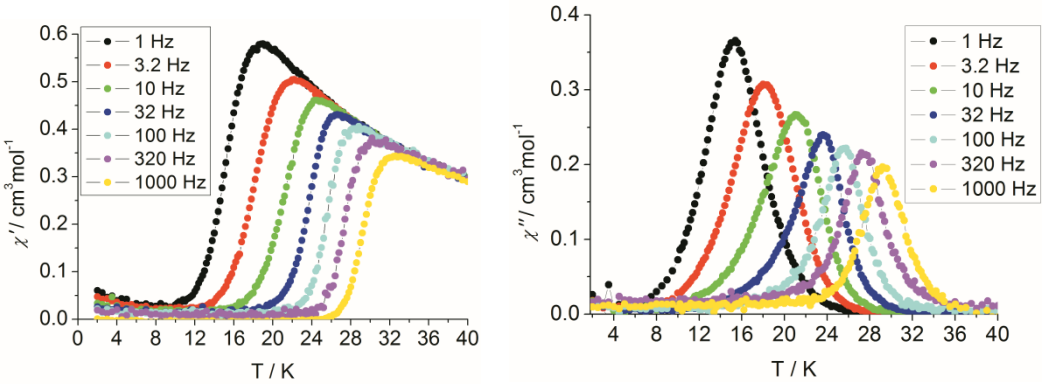

Fig. S11 The temperature dependence of the in-phase (χ') and out-of-phase (χ'') ac susceptibility under 1000 Oe dc field for **1**.

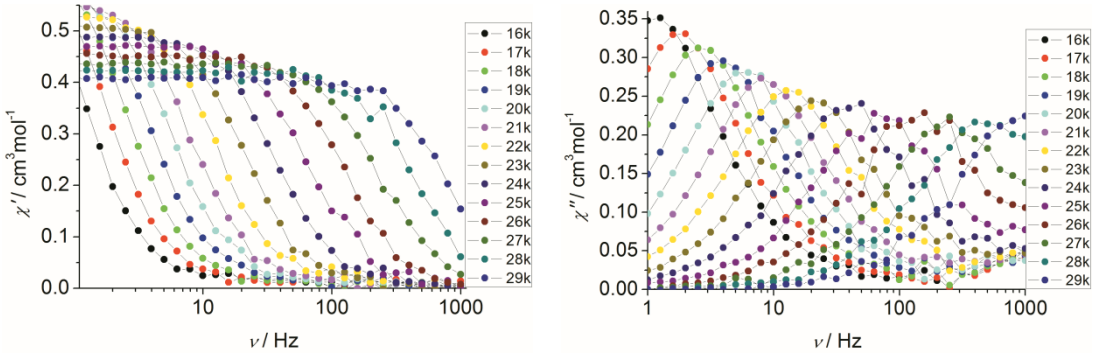

Fig. S12 The frequency dependence of the in-phase (χ') and out-of-phase (χ'') ac susceptibility under 1000 Oe dc fields for **1**.

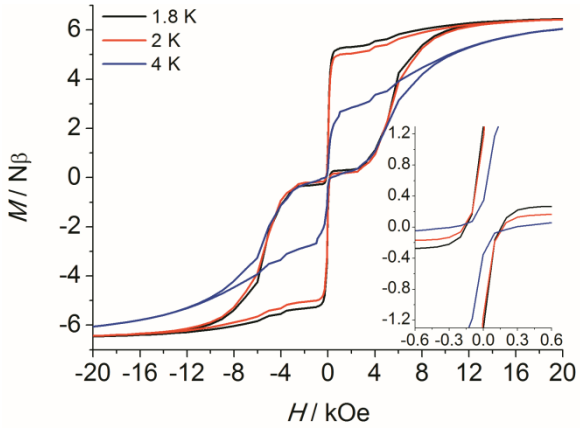

Fig. S13 The opening hysteresis loops until 4 K recorded on the sample with 20 times magnetic site dilution for **1** by a Quantum Design MPMS XL-5 SQUID magnetometer.

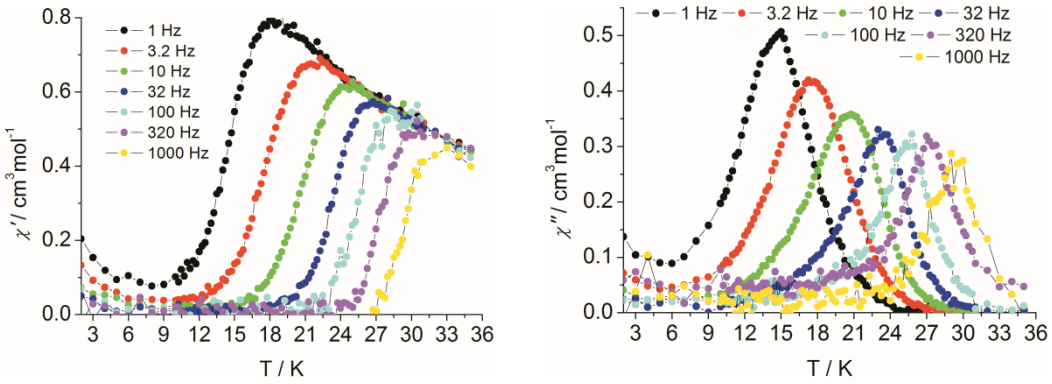

Fig. S14 The temperature dependence of the in-phase (χ') and out-of-phase (χ'') ac susceptibility under zero dc field for the sample with 20 times magnetic site dilution for **1**.

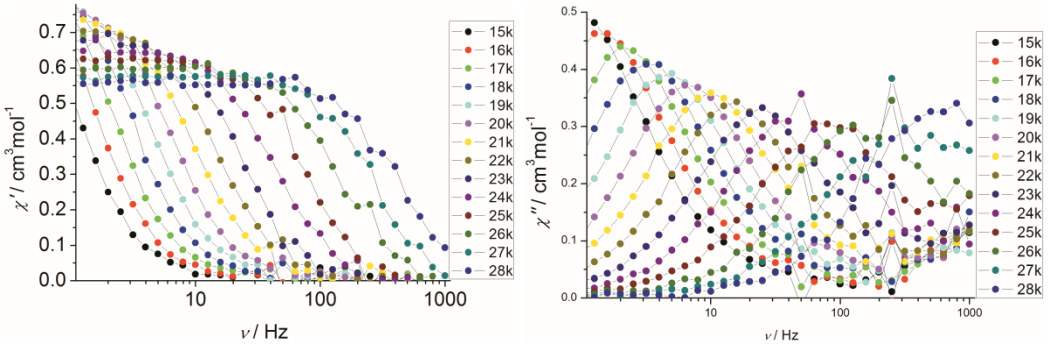

Fig. S15 The frequency dependence of the in-phase (χ') and out-of-phase (χ'') ac susceptibility under zero dc field for the sample with 20 times magnetic site dilution for **1**.